Title	Joint measurement of electron density, temperature, and emission spectrum of Nd:YAG laser-produced tin plasma
Author(s)	Pan, Y.; Tomita, K.; Sunahara, A. et al.
Citation	Applied physics letters, 123(20), 204103 https://doi.org/10.1063/5.0174185
Issue Date	2023-11-13
Doc URL	https://hdl.handle.net/2115/93519
Rights	This article may be downloaded for personal use only. Any other use requires prior permission of the author and AIP Publishing. This article appeared in Y. Pan, K. Tomita, A. Sunahara, A. Sasaki, K. Nishihara; Joint measurement of electron density, temperature, and emission spectrum of Nd:YAG laser-produced tin plasma. Appl. Phys. Lett. 13 November 2023; 123 (20): 204103 and may be found at https://doi.org/10.1063/5.0174185.
Type	journal article
File Information	204103_1_5.0174185.pdf

Applied Physics Letters

RESEARCH ARTICLE | NOVEMBER 14 2023

Joint measurement of electron density, temperature, and emission spectrum of Nd:YAG laser-produced tin plasma

Special Collection: Plasma Sources for Advanced Semiconductor Applications

Y. Pan ; K. Tomita ; A. Sunahara ; A. Sasaki ; K. Nishihara

Appl. Phys. Lett. 123, 204103 (2023)
https://doi.org/10.1063/5.0174185

Applied Physics Letters ARTICLE pubs.aip.org/aip/apl

Joint measurement of electron density, temperature, and emission spectrum of Nd:YAG laser-produced tin plasma

Cite as: Appl. Phys. Lett. **123**, 204103 (2023); doi: 10.1063/5.0174185
Submitted: 28 August 2023 · Accepted: 29 October 2023 ·
Published Online: 14 November 2023

Y. Pan,[1] K. Tomita,[1,a)] A. Sunahara,[2,3] A. Sasaki,[4] and K. Nishihara[3,5]

AFFILIATIONS

[1]Division of Quantum Science and Engineering, Graduate School of Engineering, Hokkaido University, Kita 13, Nishi 8, Kita-ku, Sapporo, Hokkaido 060-8628, Japan
[2]Center for Materials Under Extreme Environment (CMUXE), School of Nuclear Engineering, Purdue University, 500 Central Drive, West Lafayette, Indiana 47907, USA
[3]Institute of Laser Engineering, Osaka University, 2-6 Yamadaoka, Suita, Osaka 565-0871, Japan
[4]Kansai Institute for Photon Science (KPSI), National Institutes for Quantum Science and Technology (QST), 8-1 Umemidai, Kizugawa-shi, Kyoto 619-0215, Japan
[5]Faculty of Engineering, Osaka Metropolitan University, Sugimoto, Sumiyoshi, Osaka 558-8585, Japan

Note: This paper is part of the Special Topic: Plasma Sources for Advanced Semiconductor Applications.
[a)]**Author to whom correspondence should be addressed:** tomita.kentaro@eng.hokudai.ac.jp

ABSTRACT

We present the results of joint measurements of electron density (n_e), temperature (T_e), and emission spectra of an Nd:YAG-driven tin plasma. Collective Thomson scattering provides space- and time-resolved n_e and T_e data during drive laser irradiation, and extreme ultraviolet (EUV) emission spectra, which is space-resolved in the target normal, are measured using a flat-field grazing incidence spectrometer (GIS). As the distance from the target increased, the emission intensity quickly decreases, and the peaks of the spectra gradually shift to longer wavelengths. This can be explained by the rapid decrease in n_e, and thus, self-absorption, with an increase in distance. We obtain the EUV spectra by calculating the transfer of photons along the line-of-sight of the GIS, using theoretical emissivity and opacity, and applying the measured spatial distribution of n_e and T_e. The results quantitatively demonstrate that the self-absorption effect is significant; the emission from the core regions is mostly reabsorbed by the surrounding plasma. The calculated spectra are compared with the measured spectra. While good agreement is achieved in the spectral region of 13.3 and 15.3 nm, considerable differences are found in the 12.5–13 and 15.5–17.5 nm region. The results demonstrate the significance of this joint measurement for further validation of the atomic process model considering self-absorption effect, which is critical for the future high-density, solid laser-driven EUV source.

Laser-produced tin plasmas (tin-LPPs) serve as advanced light sources for state-of-the-art extreme ultraviolet (EUV) lithography.[1–3] In current industrial machines, tin-LPPs are formed by high-power CO_2-lasers operating at 10.6 μm wavelength,[4] emitting intense and narrow-band EUV emissions centered near a wavelength of 13.5 nm. Solid-state YAG lasers operating at 1.06 μm wavelength could be a promising alternative drive laser source, considering their advantages in efficiently converting electrical power to laser light.[5–8] The decrease in laser wavelength by a factor of ten results in a critical plasma density ($n_{crit} \propto \lambda^{-2}$) 100 times higher for YAG lasers, allowing penetration and absorption of laser light in higher density regions near the target surface. While this enhances the efficiency of laser absorption by the tin target, it also leads to significant self-absorption of the emitted EUV light, causing broadening of the EUV spectral emission beyond the reflective bandwidth of the available multi-layer optics[8–10] (2% centered on 13.5 nm, so-called in-band).

The electron density (n_e) and temperature (T_e) in these plasmas are critical parameters for optimizing the source output as they determine the physical processes in the EUV source, such as the laser absorption and radiative properties. Previous modeling efforts have demonstrated that EUV emissivity and opacity are directly related to the n_e and T_e in the plasma light source.[11–18] Therefore, the optimization of EUV plasma ultimately relies on determining the optimal plasma conditions that can maximize the EUV in-band output while minimizing the self-absorption effect. To this end, the plasma conditions need to be measured to provide a full view of the spatial and temporal evolution of n_e and T_e when the plasma radiates EUV light. Additionally, it is equally important to understand the spectrum of the emitted light, and thus, the complex atomic physics of highly charged Sn ions.[11,19–25] Recent studies have demonstrated that transitions between the multiply excited configurations considerably contribute to EUV emission as well as opacity.[26,27] The complexity of such processes makes the accurate modeling of the emission spectra a nontrivial task, raising the need for experimental studies. However, such studies are far from complete. While line-integrated n_e has been studied using laser interferometry,[28,29] spatially and temporally resolved n_e and T_e in tin-LPPs have rarely been measured. As a result, in most cases, n_e and T_e have to be estimated using model or simulation to explain the EUV spectra. No experimental studies covering both the plasma conditions and the resultant emission spectra have been performed on laser-produced tin plasmas.

In this Letter, we present the simultaneous measurement of the electron density, electron temperature, and emission spectrum of a YAG-driven Sn plasma. This has been possible with the combination of two experimental techniques. First, the ion-feature of collective Thomson scattering (CTS) provides space- and time-resolved plasma density and temperature data, and second, space-resolved EUV emission is measured by a flat-field grazing incidence spectrometer (GIS). Unlike earlier works,[5,7–9] we explained the EUV spectra variation using measured plasma conditions, instead of relying on analytical or simulation predictions. In addition, we obtain the EUV spectra by calculating the transfer of photons along the line-of-sight of the GIS using the theoretical emissivity and opacity[11] and the measured spatial distribution of n_e and T_e. The output spectra from the calculations are then compared with the measured spectra. This joint measurement of n_e, T_e, and EUV spectra in high-density LPP, where EUV spectra are strongly affected by self-absorption, has enabled direct experimental verification of atomic processes in tin-LPPs at high density.

In the experiment, the plasma density (n_e) and temperature (T_e) were measured with CTS, as shown in Fig. 1(a). A planar solid tin target was irradiated from its normal with a 1.06 μm Nd:YAG laser with a 7 ns pulse width in full width at half-maximum (FWHM). The spot diameter on the target surface was measured to be 550 μm (FWHM), which was slightly larger than the target thickness (0.5 mm) in the Y-direction. A laser intensity of 3×10^{10} W/cm^2 was obtained on the target. Another second harmonic, injected-seeded Nd:YAG laser with a 4 ns pulse width (FWHM) was used as the probe, creating a 50 μm spot in the plasma plume. The probe beam was arranged perpendicular to the drive laser beam in the Y-direction. The target was moved with respect to the probe beam to achieve space-resolved measurements in the X-direction. The CTS signal was observed at 45° (scattering angle of 135°) from the target normal using a custom-made spectrometer[30] equipped with an intensified charge-coupled device (ICCD) camera (1024×1024 pixels, 13 μm/pixel). The instrumental width (spectral resolution) was 18 pm, and the temporal resolution, set by the ICCD camera gate width, was 2 ns. The spatial resolution was 20 μm in the Y-direction (determined by the pixel size of ICCD) and 50 μm in X- and Z-directions (determined by the spot size of the probe laser). In this work, the time when the drive laser intensity reaches its maximum is defined as "0 ns," and the time during the drive laser irradiation is of the most interest. Figure 1(b) shows an example of the recorded CTS spectra at 0 and 130 μm above the target. In the collective scattering regime, the spectrum exhibits two ion acoustic features.[31,32] Electron temperature profiles can be extracted from the Thomson scattering signal based on the wavelength separation of the ion-acoustic feature, as described in Ref. 33. The electron density was determined by calibrating the value of the scattered power using Rayleigh scattering in air, via the following relation: $S_i(k)n_e = n_R(\sigma_R/\sigma_T)(I_T/I_R)$, where $S_i(k)$ is the frequency-integrated spectral density function; n_R is the density of the gas used in the Rayleigh calibration; I_T and I_R are the total Thomson and Rayleigh scattered intensities, respectively. The ratio of the Thomson cross section to the Rayleigh cross section (σ_R/σ_T) is well known for air under atmospheric pressure.[34] Regarding the plasma heating by the probe laser, the relative temperature increase $(\Delta T_e/T_e)$ has been well discussed in a previous paper[35] based on a model considering the absorption by the inverse bremsstrahlung and the heat transport to the volume surrounding the laser beam during the laser pulse. As a result, $\Delta T_e/T_e$ was estimated to be less than 5% in the cases reported here.

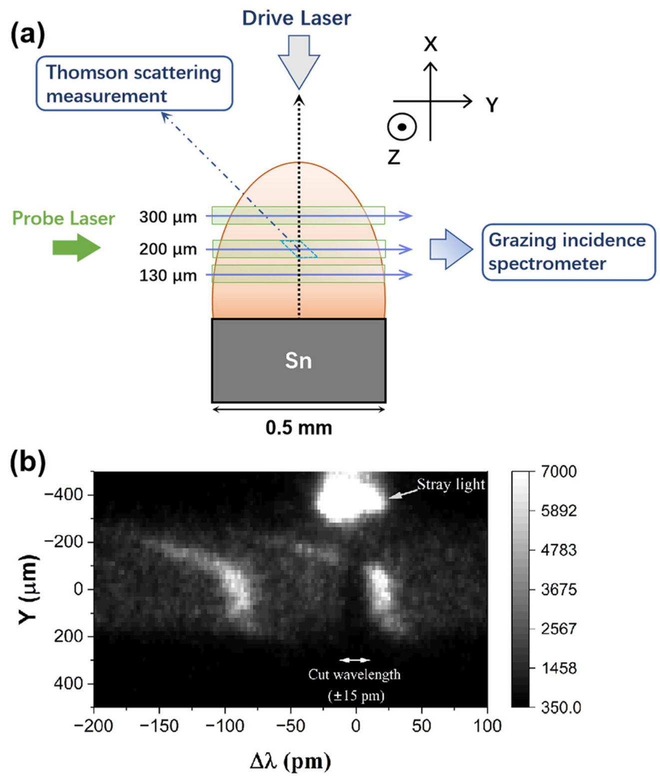

FIG. 1. (a) Sketch of the experimental setup in top view. (b) CTS spectrum obtained at 0 ns, 130 μm above the target surface.

The EUV emission spectra were measured using GIS in a separate set of experiments, where the tin-LPP was created under identical conditions, except that the target width in the Y-direction was 2 mm. Time-integrated EUV emission was observed using a GIS at 90° with respect to the drive laser beam. This GIS is equipped with an Au coated toroidal mirror (size: 50×25 mm^2), a 1200 grooves/mm flat-field grating (size: 50 × 30 mm^2), an entrance slit width of 30 μm, and a back illuminated x-ray CCD camera (1024 × 1024 pixels, 13 μm/pixel). Wavelength calibration in the 10–18 nm region was carried out through hydrogen-like and helium-like line spectra from carbon plasmas.[36] The spectral resolution was about 0.05 nm, determined mainly by the slit width and the pixel size of the camera.[37] It is worth noting that the 90° view angle and the toroidal mirror in GIS allow for a space-resolved measurement of EUV spectra in the X–Z plane with spatial resolutions of 30 μm in both X- and Z-directions, determined by the slit width and pixel size, respectively. The recorded emissions are integrated along the line-of-sight (Y-direction). The space-resolved measurement in X-direction was conducted by moving the Sn target along the target normal, in steps of 25 μm, with respect to the line-of-sight of the GIS.

In Fig. 2(a), we present the CTS-measured 2D profiles of n_e and T_e of tin-LPP, as well as their temporal evolution at time delays of 0, 2, and 4 ns. Later time delays or distances farther from the target are not of interest because tin-LPPs mainly radiate EUV light when the temperature is high. The CTS results indicate the tin plasma reached $n_e \sim 4 \times 10^{19}$ cm^{-3} and $T_e \sim 26$ eV at 0 ns, 130 μm above the target. This n_e rapidly decreases to 8×10^{18} cm^{-3} as the distance increases in the X-direction to 300 μm or in the Y-direction to 200 μm, as shown in Fig. 2(b). At the same time, T_e distributes more uniformly in space, with a small difference within ± 2 eV. After the laser peak, T_e rapidly falls over the next few nanoseconds, whereas a high n_e is maintained near the target surface. A steep decrease in n_e and uniform distribution of T_e are also observed at 2 and 4 ns.

Figure 3 shows the spaced-resolved EUV spectra in the target normal recorded by GIS, which are normalized to their respective maxima. The prominent characteristic observed in Fig. 3 is the shift in the spectral peaks from 13.1 nm toward 13.7 nm with the increasing distance from the target surface. This shift can be attributed to the decrease in optical depth at farther distances, because n_e quickly decreases with increasing distance, as shown in the upper panels in Fig. 2(a). This will be further discussed later using Fig. 4(c). We also see a quick decrease in the intensities of the spectra with increasing distance. At 130, 200, and 300 μm, the peak intensities decrease to approximately 63%, 25%, and 8% of the maximum value obtained at 25 μm, respectively.

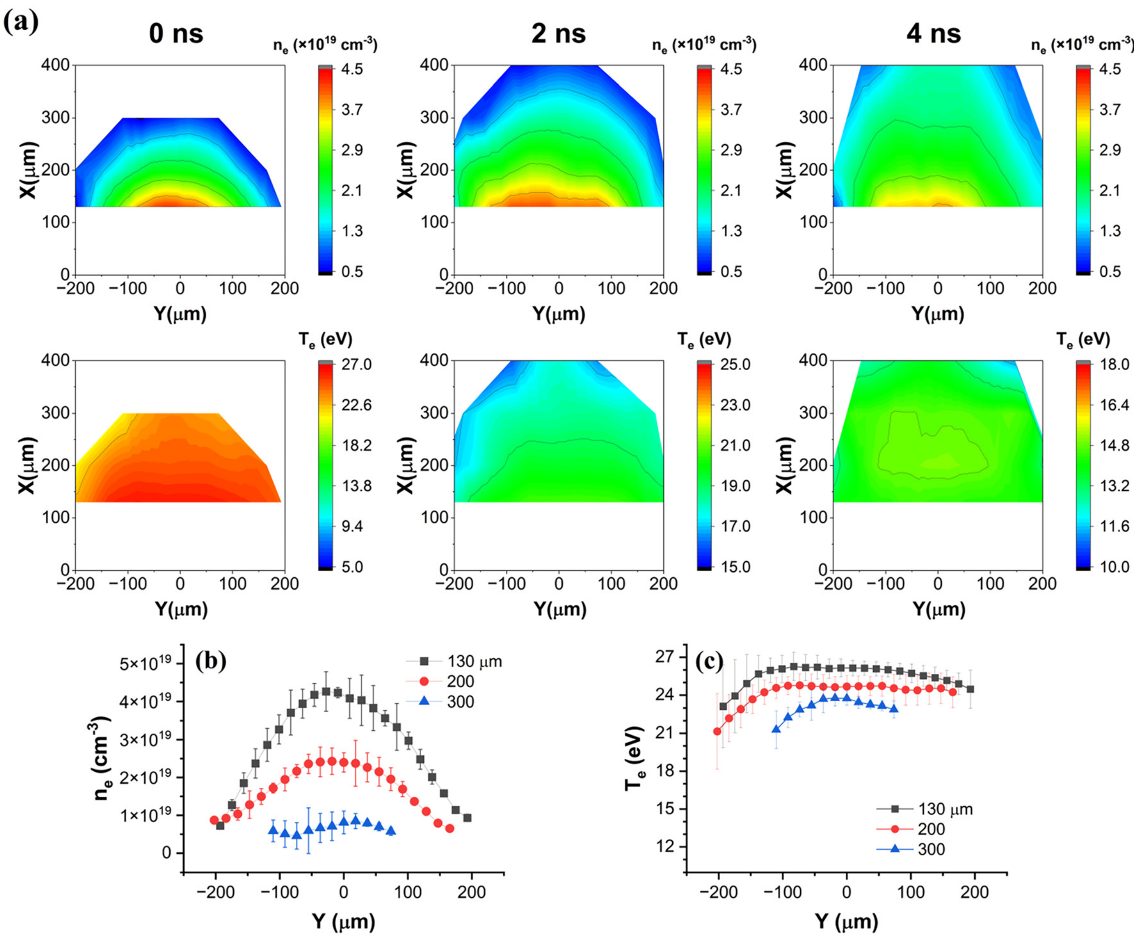

FIG. 2. (a) 2D contour plots of the CTS results. Upper panels: n_e, Lower panels: T_e. Y-distribution of n_e (b) and T_e (c) at 0 ns, 130–300 μm above the target. The error bars displayed in (b) are attributed to changes in the system sensitivity before/after the experiment, while in (c) the error bars are assigned based on the uncertainties in determining the wavelength separation of the ion-acoustic feature.

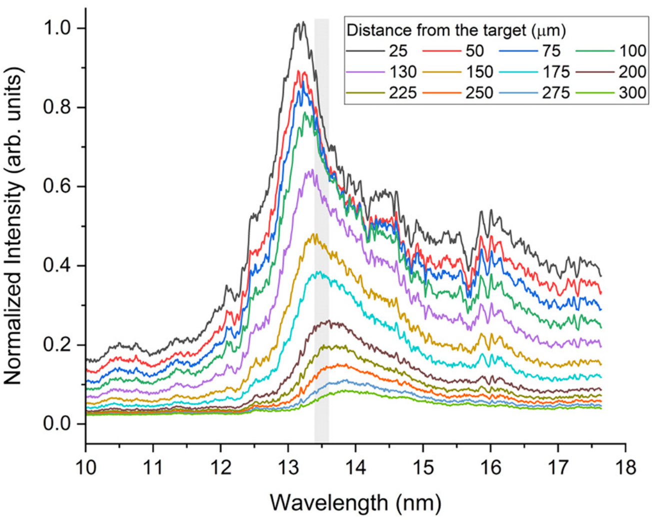

FIG. 3. Normalized emission spectra measured at multiple distances from the target. The gray-shaded area shows the 2% bandwidth around 13.5 nm (in-band wavelength).

To test the existing EUV spectrum model against the experiment, the modeled spectra are calculated by solving the photon transfer along the line-of-sight (Y+ direction), using the CTS-measured n_e and T_e given in Fig. 2(a), and the theoretical emissivity and opacity from Ref. 11. The ray trace method[38] is used to calculate the radiation transport. The calculation results, which are integrated over time (0–4 ns) and space along the line-of-sight, are given in Fig. 4(a). Two types of modeling spectra are calculated: those that consider the self-absorption effect are shown as broken lines, while those that do not are shown as solid lines. The large intensity differences between the broken and solid lines indicate strong self-absorption of the emitted radiation in this dense plasma. When self-absorption effect is not considered, the spectra look jagged due to the atomic data used in the calculation having a high resolution of about 0.05 nm. In contrast, the spectra that considered the self-absorption effect appear much smoother because, as shown in Fig. 4(c), the wavelength where strong radiation occurs also experiences significant self-absorption. It is intrusive to study how much the emission energy produced at a certain Y-location, can finally escape the plasma along Y+ direction. The results are presented in Fig. 4(b). One can see that, for 130 μm, the emission from the core, dense regions is mostly reabsorbed by the surrounding plasmas, while the observed emission feature mainly originates from the plasma at $Y > 100\ \mu$m. Because of the rapid decrease in the density along the target normal, self-absorption is significantly reduced at $X = 200$ and 300 μm, leading to an increased transmission ratio. Finally, the spectral characteristics of self-absorption are given in Fig. 4(c). At $X = 130\ \mu$m, self-absorption mainly occurs between 13.3 and 14.3 nm wavelength, with a much smaller impact at 13.3 nm or shorter wavelengths. This can explain the reason why the spectra measured at close distances, as shown in Fig. 3, have peaks near 13.3 nm. As the distance from the target increases, the absorption dip around 13.5 nm quickly weakens. In other words, a decrease in n_e considerably reduces self-absorption around 13.5 nm, while in other wavelengths, the decrease is relatively minor. As a result, the spectral peaks shift toward longer wavelengths with the increasing distance from the target, as depicted in Fig. 3.

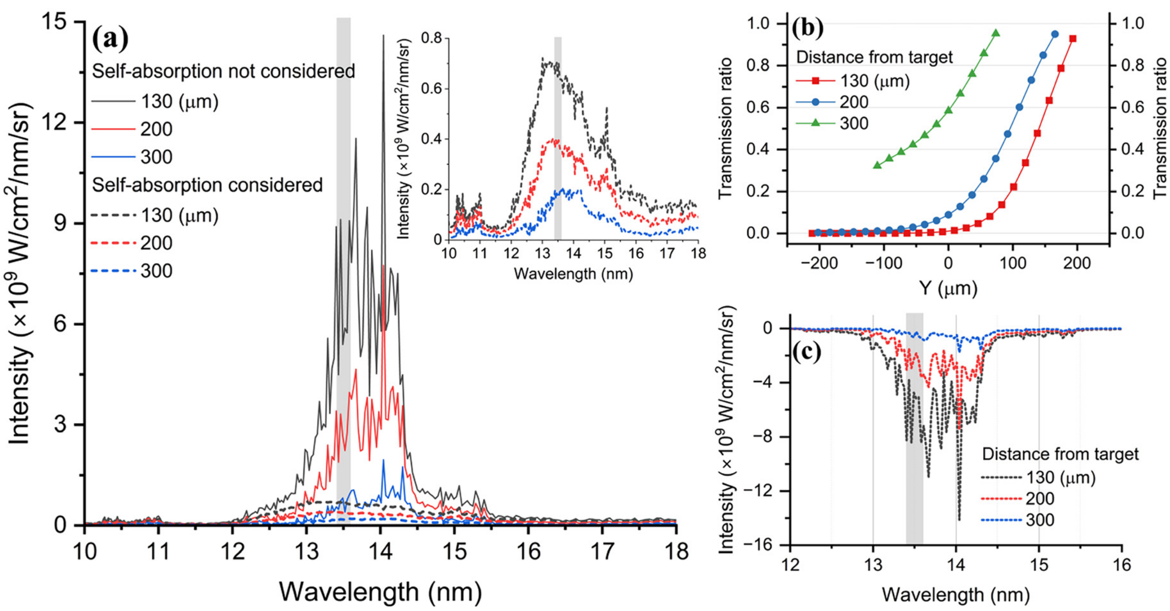

FIG. 4. (a) The modeling spectra are calculated using n_e/T_e data from CTS measurement. The spectra that consider the self-absorption effect are shown by the broken lines, while those that do not are shown in the solid lines. The gray-shaded area indicates the in-band region. Inset: Zoomed-in view of the broken lines. (b) Transmission ratio of emission, which is produced at a certain Y-position at 0 ns, along Y+ direction. The emission is integrated over time and wavelength between 10 and 18 nm. (c) The spectral features of self-absorption.

The experimental emission spectra are compared with the calculated spectra, as shown in Fig. 5. The calculated spectra, shown in black, account for the self-absorption effect. For visibility and ease of comparison, the spectra are normalized to their respective maximum values. Similar to the experimental results, the peaks of the calculated results shift to longer wavelengths as the distance from the target increases. The spectra in the region between 13.3 and 15.3 nm, including the most interested in-band wavelength, exhibit a reasonable agreement between the measured and calculated results. However, the differences in the other regions are pronounced. A prominent difference between the spectra is seen in the 12.5–13 and 15.5–17.5 nm regions. Also, it is apparent that the spectral feature peaks near 10–11 and 15 nm is missing in the measured cases. The emissivity and opacity from Ref. 11, which is used in the present calculation, was based on a relatively simple set of configurations, $4d^N$, $4d^{N-1}(4f|5p|5f)$, and $4p^54d^{N+1}$, including a limited number of multiply excited states. The calculation reproduces the spectra from CO_2 laser-driven tin plasmas with a low density, where the emission mainly arose from singly excited states. However, as addressed in a recent study,[26] in the case of YAG-driven plasmas, the excitation to multiply excited configurations increases, making a substantial contribution to the EUV emission as well as the opacity. These emissions appear on the shorter and longer wavelength sides of the main peak, which increases the spectral width of the main peak. To produce a more accurate prediction of the emission spectra from YAG-driven tin plasmas, a considerably larger number of configurations and related configuration–interactions should be considered in future modeling works.

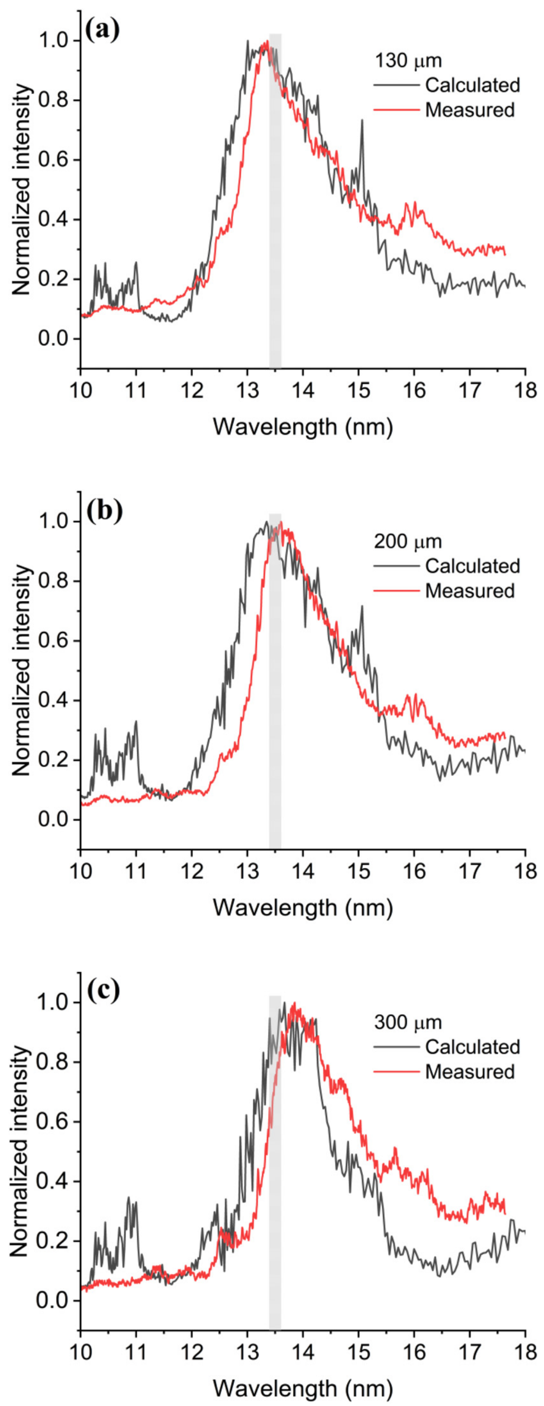

FIG. 5. The comparison between the modeled spectra and the measured spectra, at (a) 130, (b) 200, and (c) 300 μm. The gray-shaded area indicates the in-band region.

We note that a 2 mm-wide target was used in the GIS experiment, which was longer than that used in the CTS. This could potentially lead to increased reabsorption of emissions at the plasma edge in the GIS experiment. However, as shown in Fig. 2(b), due to the low density at the edge, the reabsorption effect for $Y > 200\,\mu$m is expected to be small. This may cause a reduction in the transmission ratio [Fig. 4(b)] by up to 20%. Our future work will involve measuring the plasma conditions and emission spectra under identical target and laser conditions to provide a comparison on a more equal footing.

In summary, we experimentally investigate the density, temperature, and EUV spectra of Nd:YAG-driven tin plasma and enabled a comparison between the measured spectra with those predicted by the atomic model. The CTS provides detailed time- and space-resolved density and temperature information of the plasma when the EUV light mainly radiates. Using a GIS, the emission spectrum was space-resolved in the target normal direction. With increasing distance from the target, the emission intensity quickly decreases, and the peak of the spectra gradually shift to longer wavelengths. We calculated the modeling spectra using the theoretical emissivity and opacity and the CTS-measured density and temperature. There is a significant difference in terms of the spectral shape and intensity between the calculated spectra when the self-absorption effect is considered and those when it is not. This indicates that the emitted radiation is mostly reabsorbed by the surroundings. Finally, we compared the modeled spectra with the measured spectra. While good agreement is achieved in the spectral region of 13.3 and 15.3 nm, considerable differences are found in the 12.5–13 and 15.5–17.5 nm regions. This discrepancy could be explained by the lower predictive accuracy of the atomic model, because only a limited number of multiply excited states are considered. Looking further, this approach can provide a valuable experimental benchmark for existing atomic models, assisting the refinement of more accurate and predictive models in the future.

This work was supported by the Japan Society for the Promotion of Science (JSPS) KAKENHI (Grant Nos. 23H01147 and 22KJ2443). We would like to thank Shinichi Namba and Jiahao Wang at the Hiroshima University for useful discussions.

AUTHOR DECLARATIONS

Conflict of Interest

The authors have no conflicts to disclose.

Author Contributions

Yiming Pan: Conceptualization (equal); Data curation (lead); Formal analysis (lead); Funding acquisition (supporting); Investigation (equal); Methodology (equal); Visualization (lead); Writing – original draft (lead); Writing – review & editing (equal). **Kentaro Tomita:** Conceptualization (lead); Funding acquisition (lead); Investigation (equal); Methodology (equal); Project administration (lead); Resources (lead); Supervision (lead); Validation (lead); Writing – review & editing (equal). **Atsushi Sunahara:** Data curation (equal); Formal analysis (equal); Investigation (equal); Methodology (equal); Resources (equal); Software (lead); Validation (equal); Visualization (equal); Writing – review & editing (equal). **Akira Sasaki:** Formal analysis (equal); Investigation (equal); Methodology (equal); Software (equal); Writing – review & editing (equal). **Katsunobu Nishihara:** Conceptualization (equal); Formal analysis (equal); Investigation (lead); Methodology (equal); Project administration (equal); Supervision (equal); Writing – review & editing (equal).

DATA AVAILABILITY

The data that support the findings of this study are available from the corresponding author upon reasonable request.

REFERENCES

[1] O. O. Versolato, Plasma Sources Sci. Technol. **28**, 083001 (2019).
[2] O. O. Versolato, J. Sheil, S. Witte, W. Ubachs, and R. Hoekstra, J. Opt. **24**, 054014 (2022).
[3] G. O'Sullivan, B. Li, R. D'Arcy, P. Dunne, P. Hayden, D. Kilbane, T. McCormack, H. Ohashi, F. O'Reilly, P. Sheridan, E. Sokell, C. Suzuki, and T. Higashiguchi, J. Phys. B **48**, 144025 (2015).
[4] I. Fomenkov, D. Brandt, A. Ershov, A. Schafgans, Y. Tao, G. Vaschenko, S. Rokitski, M. Kats, M. Vargas, M. Purvis, R. Rafac, B. La Fontaine, S. De Dea, A. LaForge, J. Stewart, S. Chang, M. Graham, D. Riggs, T. Taylor, M. Abraham, and D. Brown, Adv. Opt. Technol. **6**, 173 (2017).
[5] R. Schupp, F. Torretti, R. A. Meijer, M. Bayraktar, J. Scheers, D. Kurilovich, A. Bayerle, K. S. E. Eikema, S. Witte, W. Ubachs, R. Hoekstra, and O. O. Versolato, Phys. Rev. Appl. **12**, 014010 (2019).
[6] D. J. Hemminga, L. Poirier, M. M. Basko, R. Hoekstra, W. Ubachs, O. O. Versolato, and J. Sheil, Plasma Sources Sci. Technol. **30**, 105006 (2021).
[7] L. Behnke, R. Schupp, Z. Bouza, M. Bayraktar, Z. Mazzotta, R. Meijer, J. Sheil, S. Witte, W. Ubachs, R. Hoekstra, and O. O. Versolato, Opt. Express **29**, 4475 (2021).
[8] R. Schupp, F. Torretti, R. A. Meijer, M. Bayraktar, J. Sheil, J. Scheers, D. Kurilovich, A. Bayerle, A. A. Schafgans, M. Purvis, K. S. E. Eikema, S. Witte, W. Ubachs, R. Hoekstra, and O. O. Versolato, Appl. Phys. Lett. **115**, 124101 (2019).
[9] R. Schupp, L. Behnke, J. Sheil, Z. Bouza, M. Bayraktar, W. Ubachs, R. Hoekstra, and O. O. Versolato, Phys. Rev. Res. **3**, 013294 (2021).
[10] Z. Bouza, J. Byers, J. Scheers, R. Schupp, Y. Mostafa, L. Behnke, Z. Mazzotta, J. Sheil, W. Ubachs, R. Hoekstra, M. Bayraktar, and O. O. Versolato, AIP Adv. **11**, 125003 (2021).
[11] A. Sasaki, A. Sunahara, H. Furukawa, K. Nishihara, S. Fujioka, T. Nishikawa, F. Koike, H. Ohashi, and H. Tanuma, J. Appl. Phys. **107**, 113303 (2010).
[12] T. Sizyuk and A. Hassanein, Phys. Plasmas **19**, 083102 (2012).
[13] T. Sizyuk and A. Hassanein, Phys. Plasmas **22**, 093101 (2015).
[14] T. Sizyuk and A. Hassanein, Phys. Plasmas **27**, 103507 (2020).
[15] T. Sizyuk, J. Appl. Phys. **126**, 163302 (2019).
[16] M. M. Basko, V. G. Novikov, and A. S. Grushin, Phys. Plasmas **22**, 053111 (2015).
[17] M. M. Basko, Phys. Plasmas **23**, 083114 (2016).
[18] J. White, G. O'Sullivan, S. Zakharov, P. Choi, V. Zakharov, H. Nishimura, S. Fujioka, and K. Nishihara, Appl. Phys. Lett. **92**, 151501 (2008).
[19] J. Colgan, D. P. Kilcrease, J. Abdallah, M. E. Sherrill, C. J. Fontes, P. Hakel, and G. S. J. Armstrong, High Energy Density Phys. **23**, 133 (2017).
[20] R. D'Arcy, H. Ohashi, S. Suda, H. Tanuma, S. Fujioka, H. Nishimura, K. Nishihara, C. Suzuki, T. Kato, F. Koike, J. White, and G. O'Sullivan, Phys. Rev. A **79**, 042509 (2009).
[21] S. S. Churilov and A. N. Ryabtsev, Phys. Scr. **73**, 614 (2006).
[22] S. S. Churilov, R. R. Kildiyarova, A. N. Ryabtsev, and S. V. Sadovsky, Phys. Scr. **80**, 045303 (2009).
[23] A. Windberger, F. Torretti, A. Borschevsky, A. Ryabtsev, S. Dobrodey, H. Bekker, E. Eliav, U. Kaldor, W. Ubachs, R. Hoekstra, J. R. Crespo López-Urrutia, and O. O. Versolato, Phys. Rev. A **94**, 012506 (2016).
[24] Z. Bouza, J. Scheers, A. Ryabtsev, R. Schupp, L. Behnke, C. Shah, J. Sheil, M. Bayraktar, J. R. C. López-Urrutia, W. Ubachs, R. Hoekstra, and O. O. Versolato, J. Phys. B **53**, 195001 (2020).
[25] F. Torretti, A. Windberger, A. Ryabtsev, S. Dobrodey, H. Bekker, W. Ubachs, R. Hoekstra, E. V. Kahl, J. C. Berengut, J. R. C. López-Urrutia, and O. O. Versolato, Phys. Rev. A **95**, 042503 (2017).
[26] F. Torretti, J. Sheil, R. Schupp, M. M. Basko, M. Bayraktar, R. A. Meijer, S. Witte, W. Ubachs, R. Hoekstra, O. O. Versolato, A. J. Neukirch, and J. Colgan, Nat. Commun. **11**, 2334 (2020).
[27] J. Sheil, O. O. Versolato, A. J. Neukirch, and J. Colgan, J. Phys. B **54**, 035002 (2021).
[28] J. Filevich, J. J. Rocca, E. Jankowska, E. C. Hammarsten, K. Kanizay, M. C. Marconi, S. J. Moon, and V. N. Shlyaptsev, Phys. Rev. E **67**, 056409 (2003).
[29] Y. Tao, H. Nishimura, S. Fujioka, A. Sunahara, M. Nakai, T. Okuno, N. Ueda, K. Nishihara, N. Miyanaga, and Y. Izawa, Appl. Phys. Lett. **86**, 201501 (2005).
[30] K. Tomita, Y. Sato, S. Tsukiyama, T. Eguchi, K. Uchino, K. Kouge, H. Tomuro, T. Yanagida, Y. Wada, M. Kunishima, G. Soumagne, T. Kodama, H. Mizoguchi, A. Sunahara, and K. Nishihara, Sci. Rep. **7**, 12328 (2017).
[31] J. Sheffield, D. Froula, S. H. Glenzer, and N. C. Luhmann, *Plasma Scattering of Electromagnetic Radiation, Theory and Measurement Techniques*, 2nd ed. (Elsevier, Amsterdam, 2011).
[32] J. S. Ross, S. H. Glenzer, J. P. Palastro, B. B. Pollock, D. Price, G. R. Tynan, and D. H. Froula, Rev. Sci. Instrum. **81**, 10D523 (2010).
[33] Y. Pan, A. Sunahara, S. Namba, T. Higashiguchi, and K. Tomita, J. Phys. D **56**, 405203 (2023).
[34] H.-J. Kunze, in *Plasma Diagnositcs*, edited by W. Lochte-Holtgreven (North-Holland, Amsterdam, 1968), pp. 550–616.
[35] Y. Pan, K. Tomita, Y. Yamagata, A. Sunahara, and K. Nishihara, J. Phys. D **56**, 025201 (2023).
[36] A. Kramida, Y. Ralchenko, J. Reader, and NIST ASD Team, http://physics.nist.gov/asd for NIST Atomic Spectra Database (ver.5.10), National Institute of Standards and Technology, Gaithersburg, MD, 2022.
[37] C. John, "Spectroscopic study on enhancement of water-window x-ray radiation emitted from laser-produced gold plasmas," Ph.D. thesis (Hiroshima University, 2020).
[38] K. Nishihara, A. Sunahara, A. Sasaki, M. Nunami, H. Tanuma, S. Fujioka, Y. Shimada, K. Fujima, H. Furukawa, T. Kato, F. Koike, R. More, M. Murakami, T. Nishikawa, V. Zhakhovskii, K. Gamata, A. Takata, H. Ueda, H. Nishimura, Y. Izawa, N. Miyanaga, and K. Mima, Phys. Plasmas **15**, 056708 (2008).